

# Research on the Morphology of Lithium Aluminate Films Prepared by Laser Chemical Vapor Deposition

Chi Chen

School of Chemical Engineering and Pharmacy, Wuhan Institute of Technology, Wuhan, Hubei, China.

**How to cite this paper:** Chi Chen. (2023) Research on the Morphology of Lithium Aluminate Films Prepared by Laser Chemical Vapor Deposition. *Engineering Advances*, 3(4), 369-374.  
DOI: 10.26855/ea.2023.08.018

**Received:** July 18, 2023

**Accepted:** August 15, 2023

**Published:** September 11, 2023

\***Corresponding author:** Chi Chen, School of Chemical Engineering and Pharmacy, Wuhan Institute of Technology, Wuhan, Hubei, China.

## Abstract

The Li-Al-O system has three compounds of  $\text{LiAl}_5\text{O}_8$ ,  $\text{LiAlO}_2$  and  $\text{Li}_5\text{AlO}_4$ . Among them,  $\text{LiAlO}_2$  attracts increasing attention as a potential substrate for growing GaN semiconductor due to low lattice mismatch and removability. It is also of interest as a solid tritium breeding material to produce tritium fuel by the nuclear reaction of  $\text{Li}(n, \alpha)\text{T}$  in a fusion reactor, since  $\text{LiAlO}_2$  shows high-temperature stability and good compatibility with structural materials under irradiation with neutrons. Additionally,  $\text{LiAlO}_2$  is thermochemically stable even at 973 K so that it is usually used as the support for the polymer electrolyte to form the diaphragm transporting  $\text{CO}_3^{2-}$  in molten carbonate fuel cells (MCFC). In this paper, (110) and (004)-oriented  $\gamma\text{-LiAlO}_2$  films were prepared on poly-crystalline AlN substrates by laser chemical vapor deposition at deposition temperature ( $T_{\text{dep}}$ ) of 1000–1300 K, molar ratio of Li/Al ( $R_{\text{Li/Al}}$ ) of 1.0–10 and low total pressure ( $P_{\text{tot}}$ ) of 100–200 Pa. The (004)-oriented  $\gamma\text{-LiAlO}_2$  films consisted of pyramidal grains with a columnar structure while (110)-oriented  $\gamma\text{-LiAlO}_2$  films showed granular and polygonal column. The deposition rate of  $\gamma\text{-LiAlO}_2$  films reached to 60–90  $\mu\text{m h}^{-1}$ .

## Keywords

Laser CVD, morphology, orientation, film

## 1. Introduction

Lithium aluminate ( $\gamma\text{-LiAlO}_2$ ) is one of the most thermally and chemically stable Li-containing oxide compounds, and widely studied for a variety of functional materials in the electronic and nuclear energy fields [1-3]. Because of the small lattice mismatch to GaN (1.4%),  $\gamma\text{-LiAlO}_2$  is a good substrate for the GaN epitaxial growth [4-6].  $\gamma\text{-LiAlO}_2$  is also used as an electrolyte support for in a molten carbonate full cell (MCFC) due to its high stability and low solubility in molten carbonate electrolytes [7-10]. The piezoelectricity and high acoustic velocities of  $\gamma\text{-LiAlO}_2$  are attractive for the applications such as surface acoustic wave (SAW) devices for frequency filters in the wireless communication [11, 12].  $\gamma\text{-LiAlO}_2$  is promising for a tritium solid breeding material in a fusion reactor, because it is thermally and chemically stable, and shows excellent compatibility with structural materials under irradiation with neutrons at high temperatures [13-15]. Li-Al-O compounds in the forms of bulk and powder have been fabricated by solid state sintering, combustion and sol-gel methods. Compared with bulks and powders, films have characteristics of both large specific surface area and high uniformity. Large specific surface area is advantageous in catalytic reaction, humidity detection and  $\text{CO}_2$  absorption while uniformity is essential for luminescent material in display industry and for lattice match matrix. A few studies on the preparation of Li-Al-O films were reported by using rf-magnetron sputtering and atomic layer deposition (ALD). Only non-crystalline and thin Li-Al-O films (less than a few  $\mu\text{m}$  thick) have been fabricated because of low deposition rates ranging from 0.1 to 1  $\mu\text{m h}^{-1}$ .

Solid state reaction and wet-chemical method such as sol-gel [16] have been used to prepare  $\gamma\text{-LiAlO}_2$ . However,

reports on the preparation of  $\gamma$ -LiAlO<sub>2</sub> films are limited to date.  $\gamma$ -LiAlO<sub>2</sub> film can be attractive for a buffer layer of epitaxial growth of semiconductor films and a protective layer against the corrosion of the supports and frames by the molten carbonates in MCFC [17-19]. The orientation and microstructure of the films are important factors for the epitaxial growth and resistance to the corrosion. Chemical vapor deposition (CVD) is a common industrial process to produce high-purity and high-performance solid materials such as  $\alpha$ -Al<sub>2</sub>O<sub>3</sub>. To date, it has never been used for deposition of Li-Al-O and Na-Al-O films. Chemical vapor deposition (CVD) may prepare crystalline Li-Al-O and Na-Al-O films, but the deposition rate is usually low. We have developed laser-assisted CVD (LCVD) using high-power continuous-wave oscillation laser expanded to wide deposition area with a lens. The laser irradiation field during CVD enables us to fabricate films with highly-textured microstructures at high deposition rates. We reported the high-speed growth of films in various pseudo binary systems, such as BaO–TiO<sub>2</sub> and ZrO<sub>2</sub>–Al<sub>2</sub>O<sub>3</sub>, clarifying those phase formation relationships and microstructures by LCVD. We also reported the preparation of Li-Al-O films, such as LiAl<sub>5</sub>O<sub>8</sub> and Li<sub>5</sub>AlO<sub>4</sub>, at high deposition rates by laser chemical vapor deposition (LCVD). In the present study, we report highly (110) and (004)-oriented LiAlO<sub>2</sub> film having well-crystallized and faceted texture prepared by LCVD.

## 2. Experiment

A continuous wave diode laser (InGaAlAs, wavelength: 808 nm) was employed with laser power output ( $P_L$ ) from 50 to 200 W and irradiation spot size of 15 mm in a diameter. AlN substrate (10 mm × 10 mm × 1 mm) was put on a hot stage pre-heated at 873 K ( $T_{pre}$ ). The temperature distribution in the substrate was within several K. The deposition temperature ( $T_{dep}$ ) was measured by a thermocouple beneath the substrate. The vaporization temperature ( $T_{vap}$ ) of aluminum acetylacetonate (Al(acac)<sub>3</sub>) precursor was fixed at 443 K, while that of lithium dipivaloymethanate (Li(dpm)) precursor was changed from 513 to 553 K. The molar ratio of evaporated Li to Al precursor ( $R_{Li/Al}$ ) was regulated by changing the  $T_{vap}$  of Li(dpm) precursor. The precursor vapors and O<sub>2</sub> gas were separately introduced into the reaction chamber through a double-tube nozzle. The flow rates of Ar carrier gas for each precursor and O<sub>2</sub> gas were fixed at  $8.3 \times 10^{-7}$  and  $1.7 \times 10^{-6}$  m<sup>3</sup> s<sup>-1</sup>, respectively. The temperature of all the gas lines was maintained at 553 K to prevent the condensation of precursor vapors during the transportation. The total pressure ( $P_{tot}$ ) in the reaction chamber was changed from 100 to 800 Pa. The deposition time was 600 s. The schematic of the LCVD apparatus was shown elsewhere [20-22].

The deposition rate ( $R_{dep}$ ) was calculated from the film thickness per deposition time. The crystalline phase was examined by X-ray diffraction (XRD; Rigaku: RAD-2C). The microstructure was observed by scanning electron microscopy (SEM; Hitachi: S-3100H) and FE-SEM. The degree of orientation on (hkl) reflection was calculated by the Harris texture coefficient (TC):

$$TC(hkl) = N \frac{I_m(hkl)/I_0(hkl)}{\sum I_m(hkl)/I_0(hkl)}$$

where (hkl) correspond to (110) and (004) planes of LiAlO<sub>2</sub> films.  $I_m$  and  $I_0$  are the intensity from the corresponding plane measured in the present study and that reported in JCPDS card (JCPDF#75-0905), respectively. (101), (110), (111), (200), (211), (310), (004), (302), (321) and (330) reflections of LiAlO<sub>2</sub> were used for the calculation ( $N = 10$ ).

## 3. Results and discussion

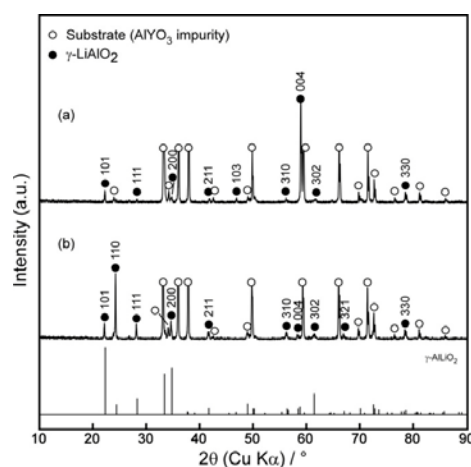


**Figure 1.** XRD patterns of  $\gamma$ -LiAlO<sub>2</sub> film prepared at  $T_{dep} = 1100$  K,  $P_{tot} = 200$  Pa and different molar ratios of Li/Al of  $R_{Li/Al} = 1.0$ (a) and  $R_{Li/Al} = 2.0$  (b).

Figure 1 shows XRD patterns of  $\gamma$ -LiAlO<sub>2</sub> film prepared at  $T_{\text{dep}} = 1100$  K,  $P_{\text{tot}} = 200$  Pa and different molar ratios of Li/Al of  $R_{\text{Li/Al}} = 1.0$  (a) and  $R_{\text{Li/Al}} = 2.0$  (b). In fig.1(a), Relative intensity of the (004) reflection peak at 58.9° was significantly higher than that of a powder pattern (JCPDF#75-0905), implying the (004) orientation. The TC value of the (004) orientation was 9.4. And the film prepared at  $R_{\text{Li/Al}} = 2.0$  had a (110)-orientation, as shown in fig.1(b), presenting a TC(110) of 9.2.

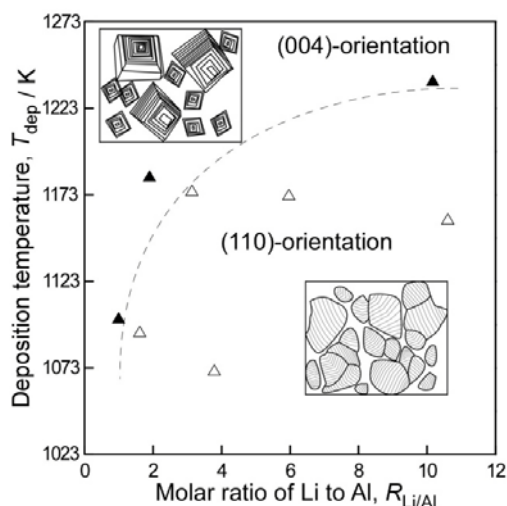


**Figure 2.** Effects of  $T_{\text{dep}}$  and  $R_{\text{Li/Al}}$  on the orientation and microstructure of  $\gamma$ -LiAlO<sub>2</sub> films prepared by laser CVD.

Fig. 2 shows the effects of  $T_{\text{dep}}$  and  $R_{\text{Li/Al}}$  on the orientation of  $\gamma$ -LiAlO<sub>2</sub> films.  $\gamma$ -LiAlO<sub>2</sub> films in a single phase were prepared at  $T_{\text{dep}} = 1000$ –1300 K,  $R_{\text{Li/Al}} = 1.0$ –10.6 and  $P_{\text{tot}} = 200$  Pa. At  $T_{\text{dep}} = 1000$ –1100 K ( $P_L = 100$  W),  $\gamma$ -LiAlO<sub>2</sub> film with (004) orientation was deposited at  $R_{\text{Li/Al}} = 1.0$ . At  $T_{\text{dep}} = 1158$ –1183 K ( $P_L = 150$  W), (004)-oriented  $\gamma$ -LiAlO<sub>2</sub> film was prepared at  $R_{\text{Li/Al}} = 2.0$ . At  $T_{\text{dep}} = 1238$  K, (004)-oriented film was obtained at  $R_{\text{Li/Al}} = 10.2$ . Thus, (004)-oriented films generally formed at relatively low  $R_{\text{Li/Al}}$  and high  $T_{\text{dep}}$ . In contrast, (110)-oriented films can be obtained at relatively high  $R_{\text{Li/Al}}$  and low  $T_{\text{dep}}$ .

The surface and cross section of  $\gamma$ -LiAlO<sub>2</sub> film with different orientations were depicted in Fig. 3. The (004)-oriented film consisted of pyramidal grains in the grain sizes of about 1–3  $\mu\text{m}$  and the cross section was columnar structure. The (110)-oriented film had granular and polygonal surface and columnar cross-section. The deposition rates of these  $\gamma$ -LiAlO<sub>2</sub> films were 60–90  $\mu\text{m h}^{-1}$ .

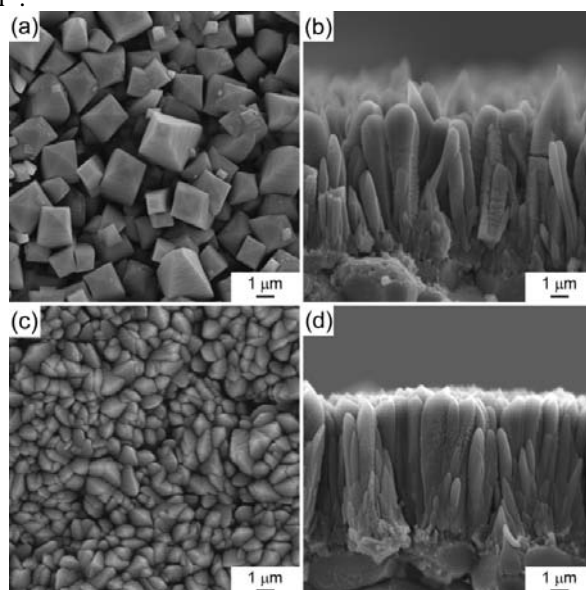


**Figure 3.** The surface and cross section of  $\gamma$ -LiAlO<sub>2</sub> film with (004)-orientation (a, b) and (110)-orientation (c, d).

Figure 4 (a) shows the FE-SEM image of the top surface of the (004)-oriented  $\gamma$ -LiAlO<sub>2</sub> film. LiAlO<sub>2</sub> has two types of structure,  $\alpha$ : hexagonal caswellsilverite (NaCrS<sub>2</sub>)-type and  $\gamma$ : tetragonal wurtzite-type. In the present study,  $\gamma$ -LiAlO<sub>2</sub> was obtained at  $R_{\text{Li/Al}} > 0.5$  and  $T_{\text{dep}} > 900$  K. These are also in agreement with the phase diagram.  $\gamma$ -LiAlO<sub>2</sub> has a wurtzite structure in a tetragonal cell ( $P4_1212$ ;  $a = 5.17$  nm and  $c = 6.295$  nm), which is composed of Al- and Li-centered tetrahedral. Each tetrahedron shares one of its edges with another tetrahedron of a different type, and each vertex of every tetrahedron is shared with two additional tetrahedra. The edge-sharing couples of Al- and Li-centered tetrahedra are aligned on (001) planes. This directional alignment of the edge-sharing couples of tetrahedra could be associated with the preferred (004) orientation in the  $\gamma$ -LiAlO<sub>2</sub> films. Compared with LiAlO<sub>2</sub>, the other two phases of LiAl<sub>5</sub>O<sub>8</sub> and Li<sub>5</sub>AlO<sub>4</sub> have different structures. LiAl<sub>5</sub>O<sub>8</sub> has two structures, i.e.,  $\alpha$ : ordered spinel and  $\beta$ : disordered spinel with no ordering between Li<sup>+</sup> and Al<sup>3+</sup> in the octahedral sites. The crystal structure of  $\alpha$ -LiAl<sub>5</sub>O<sub>8</sub> is an inverse spinel with a cubic lattice (space group:  $P4332$ , lattice constant:  $a = 7.908$  nm). The Li atoms and half of the Al atoms form six-coordinated octahedra sharing their edges. The other Al atoms form four-coordinated tetrahedra sharing corners of the octahedra. The phase of  $\alpha$ -LiAl<sub>5</sub>O<sub>8</sub> with a Li-poor and Al-rich composition is situated next to Li- $\beta$ -alumina in the phase diagram of the Al<sub>2</sub>O<sub>3</sub>-Li<sub>2</sub>O system. Among the many polymorphs of alumina,  $\gamma$ -alumina has a defective spinel where Al atoms at tetrahedral and octahedral sites are designated as Al1 and Al2, respectively. The occupancy of the octahedral Al2 site is 0.83 to satisfy the Al<sub>2</sub>O<sub>3</sub> stoichiometry in a spinel cubic cell. The crystal structure of  $\alpha$ -LiAl<sub>5</sub>O<sub>8</sub> can be understood as a derivative form of  $\gamma$ -Al<sub>2</sub>O<sub>3</sub> with substitution of the Li-centered octahedra for a quarter of the Al2-centered ones. Single-phase  $\alpha$ -LiAl<sub>5</sub>O<sub>8</sub> was obtained at  $T_{\text{dep}} = 1089$ – $1273$  K and  $R_{\text{Li/Al}} > 0.2$ . This is in agreement with the phase diagram. At higher  $T_{\text{dep}}$  values, a higher Li content was needed to obtain single-phase compounds probably due to a premature reaction of the Li (dpm) precursor in the gas phase. Meanwhile, Li<sub>5</sub>AlO<sub>4</sub> also has two types of structure,  $\alpha$ : antifluorite and  $\beta$ : antifluorite with greater disorder of the cations and vacancies in the tetrahedral sites. Single-phase  $\beta$ -Li<sub>5</sub>AlO<sub>4</sub> was obtained at  $R_{\text{Li/Al}} > 10$ , which was higher than that for the phase diagram of  $R_{\text{Li/Al}} > 5$ . This could also have been caused by the premature reaction and depletion of the Li precursor in a gas phase.  $\beta$ -Li<sub>5</sub>AlO<sub>4</sub> has a defective antifluorite structure ( $Pmmn$ ;  $a = 6.42$  nm,  $b = 6.302$  nm, and  $c = 4.62$  nm), which is derivative form of the cubic antifluorite structure of Li<sub>2</sub>O. In the cubic antifluorite structure of Li<sub>2</sub>O, Li-centered tetrahedra with O atoms occupying the face-centered sites form an edge-sharing network. Compared with the crystal structures of Li<sub>2</sub>O, the structure of  $\beta$ -Li<sub>5</sub>AlO<sub>4</sub> is analogous to that of Li<sub>2</sub>O. The substitution of Al ions by Li ions at the center of the tetrahedra results in the formation of tetrahedral anion vacancies to satisfy charge compensation, accompanied by orthorhombic distortion from the cubic symmetry. In this FE-SEM, the angles at the top of the pyramidally faceted columnar grains were about 33° and 100°.  $\gamma$ -LiAlO<sub>2</sub> has a wurtzite structure in a tetragonal symmetry ( $P4_1212$ ;  $a = 5.17$  nm and  $c = 6.295$  nm) composed of Al- and Li-centered tetrahedral [23]. Each tetrahedron shares one of its edges with another tetrahedron of different kinds and each vertex of every tetrahedron are shared with two additional tetrahedra. The angles at the top of pyramidal facets were consistent with the dihedral angles composed of {112} (100°) and {221} (33°) planes, as shown in Fig. 4 (b, c). Thus, the pyramidally faceted textures of (004)-oriented grains could be caused of the preferential growth of the {112} and {221} planes of  $\gamma$ -LiAlO<sub>2</sub>.

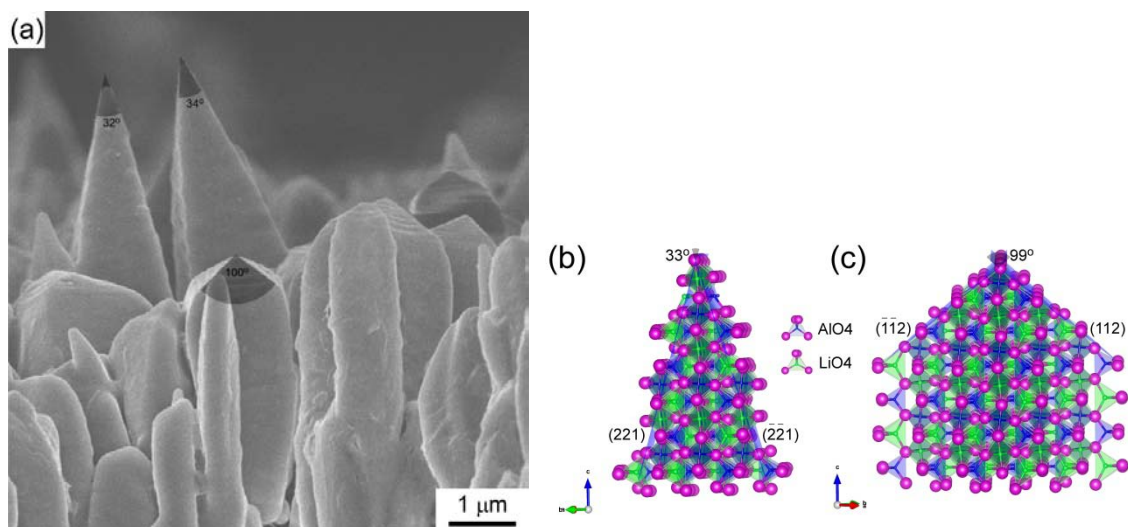


**Figure 4.** FE-SEM image of (004)-oriented  $\gamma$ -LiAlO<sub>2</sub> film (a) and crystal structure of  $\gamma$ -LiAlO<sub>2</sub> cleaved by {221} (b) and {112} planes (c).

## 4. Conclusion

$\gamma$ -LiAlO<sub>2</sub> films were prepared by laser chemical vapor deposition at  $T_{\text{dep}} = 1000\text{--}1300$  K,  $R_{\text{Li/Al}} = 1.0\text{--}10.6$  and  $P_{\text{tot}} = 100\text{--}800$  Pa. (004)-oriented films were deposited at higher  $T_{\text{dep}}$  and lower  $R_{\text{Li/Al}}$  while (110)-oriented films were fabricated at relatively lower  $T_{\text{dep}}$  and higher  $R_{\text{Li/Al}}$ . (004)-oriented films consisted of columnar grains with pyramidal caps. (110)-oriented films had granular and polygonal caps. The  $R_{\text{dep}}$  of as-prepared  $\gamma$ -LiAlO<sub>2</sub> films reached  $60\text{--}90$  m h<sup>-1</sup>. From structural analysis, the pyramidal grains of (004)-oriented  $\gamma$ -LiAlO<sub>2</sub> films were caused of the preferential growth along  $c$ -axis and low growth rate of the {112} and {221} planes.

## Acknowledgments

This work was supported by the project of Research on Preparation and Properties of Ceramic Electrolyte BASE (No. 005351), financed by Education Department of Hubei Province, China.

## References

- [1] Jianfei Jia, Bing Guo, Qinghe Zhang, Zhongbo Zhang. Grinding performance and acoustic emissions of structured CVD diamond micro-grinding tools. *Journal of Materials Processing Technology*, 318 (2023), 202-212.
- [2] Balaram Paudel Jaisi, Rucheng Zhu, Golap Kalita, Masayoshi Umeno, Morphological changes of carbon thin films with nitrogen doping synthesized by microwave-excited surface wave plasma CVD. *Materials Chemistry and Physics*, 307(2023), 399-408.
- [3] Liying Wu, Lianchang Qiu, Fangfang Zeng, Qiang Lu. Influence of deposition pressure on the microstructure and mechanical properties of CVD TiAlSiN coatings. *Surface and Coatings Technology*, 466 (2023), 1088-1092.
- [4] Mengyang Feng, Peng Jin, Xianquan Meng. One-step growth of a nearly 2 mm thick CVD single crystal diamond with an enlarged surface by optimizing the substrate holder structure. *Journal of Crystal Growth*, 603 (2023), 95-98.
- [5] Qizhong Li, Yixuan Zhang, Baifeng Ji. Improvement of SiC deposition uniformity in CVD reactor by showerhead with baffle. *Journal of Crystal Growth*, 615 (2023), 878-882.
- [6] H.J. Choi, J.J. Lee, S.H. Hyun, H.C. Lim. Submicron  $\gamma$ -LiAlO<sub>2</sub> Powder Synthesized from Boehmite. *Fuel Cells*, 9 (2009), 605-612.
- [7] L. Suski, M. Tarniowy. Determination of open-circuit potentials at gas/electrode/YSZ boundary versus molten carbonate reference electrode at medium temperatures: I. Potentials of Au and Pt in O<sub>2</sub> and H<sub>2</sub>+H<sub>2</sub>O atmospheres. *J. Mater. Sci.*, 36 (2001), 5119-5124.
- [8] K. Kinoshita, G.H. Kucera. Enthalpies of formation of liquid and solid binary alloys based on 3d metals: V. Alloys of nickel. *J. Electrochem. Soc.*, 129 (1982), 216-220.
- [9] A.V. Sotnikov, H. Schmidt, M. Wehnacht, E.P. Smirnova, T.Y. Chemekova, Y.N. Makarov. Thermoelectric properties of SmS@Y<sub>2</sub>O<sub>3</sub> and Y<sub>2</sub>O<sub>3</sub>@SmS compounds with a core-shell nanostructure. *IEEE Trans. Ultrason. Ferroelectr. Freq. Control*, 57 (2010), 808-811.
- [10] Y. Takagaki, E. Chilla, K.H. Ploog. Constituent substitution in hot wall deposition of Bi<sub>2</sub>S<sub>3</sub> films by reaction with substrates. *J. Appl. Phys.*, 97 (2005), 034902.
- [11] J. Lin, Z. Wen, X. Xu, N. Li, S. Song. Advances in Micro-Droplets Coalescence Using Microfluidics. *Fusion Eng. Des.*, 85 (2010), 1162-1166.
- [12] F. Botter, B. Rasneur, E. Roth. Irradiation behaviour of a tritium breeding material,  $\gamma$ -LiAlO<sub>2</sub>- results of two in-pile experiments: ALICE I and ALICE II. *J. Nucl. Mater.*, 160 (1988), 48-57.
- [13] F. Alessandrini, C. Alvani, S. Casadio, M.R. Mancini, C.A. Nannetti, In-situ tritium release (CORELLI-2 experiment) and ex-reactor ionic conductivity of substoichiometric LiAlO<sub>2</sub> breeder ceramics. *J. Nucl. Mater.*, 224 (1995), 236-244.
- [14] J.A. Shearer, S.W. Tam, C.E. Johnson. The enthalpies of formation of MgAl<sub>2</sub>O<sub>4</sub>, MgSiO<sub>3</sub>, Mg<sub>2</sub>SiO<sub>4</sub> and Al<sub>2</sub>SiO<sub>5</sub> by oxide melt solution calorimetry. Conference: ANS annual meeting, Detroit, MI, USA, 12 Jun 1983.
- [15] M.A. Valenzuela, J. Jimenez-Becerril, P. Bosch, S. Bulbulian, V.H. Lara. Ni and Ni<sub>3</sub>C catalysts supported on mesoporous silica for dry reforming of methane. *J. Am. Ceram. Soc.*, 79 (1996), 455-460.
- [16] T. Frianeza-Kullberg, D. McDonald, K. Davis, Standardizing Scoring Conventions for Crohn's Disease Endoscopy: An International RAND/UCLA Appropriateness Study. *Ceram. Trans.*, 12 (1990), 147.
- [17] C. Alvanic, S. Casadio. Effect of Long-Term Testosterone Administration on the Endometrium of Female-to-Male (FtM) Transsexuals. EP235099 (1987).
- [18] K.W Sang, S Binpark, et al. CePO<sub>4</sub> Coated LiNi<sub>0.6</sub>Co<sub>0.2</sub>Mn<sub>0.2</sub>O<sub>2</sub> as Cathode Material and its Electrochemical Performance. *J.*

- Nucl. Mater., 257 (1998), 172.
- [19] L.M. Carrera, J. Jimenez-Becerril, P. Bosch, S. Bulbulian. Atmospheric agro-industrial sugarcane emissions: Its effect on health and properties of the habitants. *J. Am. Ceram. Soc.*, 78 (1995), 933-938.
- [20] C. Chi, H. Katsui, R. Tu, T. Goto. Preparation of Li–Al–O films by laser chemical vapor deposition. *Mater. Chem. Phys.*, 143 (2014), 1338-1343.
- [21] S. Zhang, R. Tu, T. Goto. High-speed Epitaxial Growth of (110) SrTiO<sub>3</sub> Films on (110) MgAl<sub>2</sub>O<sub>4</sub> Substrates using Laser Chemical Vapour Deposition. *J. Am. Ceram. Soc.*, 95 (2012), 2782-2784.
- [22] K. Momma, F. Izumi. Synthesis, Crystal Structure, Ca<sup>2+</sup> and Proton Conduction Pathways of New Triphosphate Ca<sup>0.5</sup>FeHP<sub>3</sub>O<sub>10</sub>. *J. Appl. Cryst.*, 44 (2011), 1272-1276.
- [23] M. Marezio. Mechanically stimulated thermal synthesis of lithium aluminates. *Acta Crystallogr.*, 19 (1965), 396-400.